

Article

In Situ Solidified Gel Polymer Electrolytes for Stable Solid–State Lithium Batteries at High Temperatures

Junfeng Ma ^{1,2}, Zhiyan Wang ², Jinghua Wu ², Zhi Gu ², Xing Xin ¹ and Xiayin Yao ^{2,3,*}¹ School of Material Science and Chemical Engineering, Ningbo University, Ningbo 315211, China² Ningbo Institute of Materials Technology and Engineering, Chinese Academy of Sciences, Ningbo 315201, China³ Center of Materials Science and Optoelectronics Engineering, University of Chinese Academy of Sciences, Beijing 100049, China

* Correspondence: yaoxy@nimte.ac.cn

Abstract: Lithium metal batteries have attracted much attention due to their high energy density. However, the critical safety issues and chemical instability of conventional liquid electrolytes in lithium metal batteries significantly limit their practical application. Herein, we propose polyethylene (PE)–based gel polymer electrolytes by in situ polymerization, which comprise a PE skeleton, polyethylene glycol and lithium bis(trifluoromethylsulfonyl)imide as well as liquid carbonate electrolytes. The obtained PE–based gel polymer electrolyte exhibits good interfacial compatibility with electrodes, high ion conductivity, and wide electrochemical window at high temperatures. Moreover, the assembled LiFePO₄//Li solid–state batteries employing PE–based gel polymer electrolyte with 50% liquid carbonate electrolytes deliver good rate performance and excellent cyclic life at both 60 °C and 80 °C. In particular, they achieve high specific capacities of 158.5 mA h g^{−1} with a retention of 98.87% after 100 cycles under 80 °C at 0.5 C. The in situ solidified method for preparing PE–based gel polymer electrolytes proposes a feasible approach for the practical application of lithium metal batteries.

Keywords: in situ gel electrolyte; lithium metal battery; polymer electrolyte

Citation: Ma, J.; Wang, Z.; Wu, J.; Gu, Z.; Xin, X.; Yao, X. In Situ Solidified Gel Polymer Electrolytes for Stable Solid–State Lithium Batteries at High Temperatures. *Batteries* **2023**, *9*, 28. <https://doi.org/10.3390/batteries9010028>

Academic Editor: Claudio Gerbaldi

Received: 6 December 2022

Revised: 25 December 2022

Accepted: 28 December 2022

Published: 30 December 2022



Copyright: © 2022 by the authors. Licensee MDPI, Basel, Switzerland. This article is an open access article distributed under the terms and conditions of the Creative Commons Attribution (CC BY) license (<https://creativecommons.org/licenses/by/4.0/>).

1. Introduction

Over the past 30 years, rechargeable lithium–ion batteries have had tremendous success. With the demand for high energy density, lithium metal batteries have attracted widespread attention due to the high theoretical specific capacity of lithium as well as its lowest electrochemical potential [1–5]. However, organic liquid electrolyte–based lithium metal batteries usually exhibit dendritic structural evolution and continuous parasitic reactions at the electrode–electrolyte interface, leading to safety issues and low coulombic efficiency [6–10]. Significant efforts have been made to overcome these challenges, of which the exploration of safe and stable electrolytes compatible with lithium metal is particularly critical and indispensable [11–17]. Solid–state electrolytes with high stability have been considered as optional alternatives to conventional liquid electrolytes for achieving safer and more stable energy storage systems [18–20].

Among various solid electrolytes, gel polymer electrolytes with liquid organic electrolytes possess high ionic conductivity under room temperature and can form a flexible interface with the electrode [21–24]. Generally, the polymer films of gel polymer electrolytes are prepared by an ex situ method and then immersed in a liquid electrolyte for gelation. However, the gel polymer electrolyte only contacts with the top of the electrode and therefore the entire mass of active material cannot be directly utilized. Thus, additional liquid electrolyte is still required to ensure interfacial wettability when utilizing ex situ prepared gel polymer electrolytes [25,26].

In situ preparation of gel polymer electrolytes is considered a feasible method to address the aforementioned interfacial problems and active material utilization issues [27–32]. Gelation could be achieved in the presence of liquid electrolyte-containing monomers injected into the battery. This method takes advantage of low viscosity, ease of handling, and good wettability, which enable gel polymer electrolytes with enhanced interfacial contact with electrodes, creating well-connected pathways for ionic transport [27,29,31].

Herein, we present polyethylene (PE)-based gel polymer electrolytes composed of PE skeleton, polyethylene glycol (PEG), lithium bis(trifluoromethylsulfonyl)imide and liquid carbonate electrolyte (LCE) for high temperature solid-state lithium metal batteries. Poly(ethylene glycol) methyl ether acrylate (PEGMEA) is used as the monomers for in situ polymerization due to the formed PEG possessing good compatibility with lithium metal as well as high ionic conductivity [19], which enables the obtained gel polymer electrolyte to possess both good chemical stability and high ion conductivity at high temperatures. The PE-based gel polymer electrolyte with 50% liquid carbonate electrolytes (PE-50%LCE@PEG) shows a high ionic conductivity of $1.73 \times 10^{-4} \text{ S cm}^{-1}$ under 60 °C and good electrochemical stability with the lithium metal anode. The PE-50%LCE@PEG-based Li-Li symmetrical battery exhibits cycling stability for 1200 h at 0.1 mA cm⁻² and 0.1 mAh cm⁻² at 60 °C. Furthermore, the LiFePO₄/PE-50%LCE@PEG/Li cell exhibits excellent cyclic performance with no capacity decay over 150 cycles at 0.5 C under 60 °C. In addition, the cell shows a high initial reversible capacity of 160.3 mA h g⁻¹ under a higher temperature of 80 °C at 0.5 C and delivers excellent cycling stability for 100 cycles. This in situ solidified PE-based gel polymer electrolyte exhibits promising potential application in lithium metal batteries.

2. Experimental Section

2.1. Synthesis of PE-Based Gel Polymer Electrolytes

Lithium bis(trifluoromethylsulfonyl)imide (LiTFSI, Sigma) and polyethylene glycol methyl ether acrylate (Sigma, 480 g mol⁻¹) monomer with dibenzoyl peroxide (Aladdin) initiator were mixed to form a homogeneous solution. The EO:Li ratio was controlled at 18:1 and the mass of initiator was 0.2% of PEGMEA. At the same time, a LCE solution of 1 M LiPF₆ in EC/DMC/EMC (1/1/1, v/v/v) was also prepared. The gel polymer electrolyte liquid precursor solutions were prepared by mixing different amounts of LCE ($x = 40\%$, 50%, 60%) with the PEGMEA/LiTFSI solution, where x is the mass percent of PEGMEA. Then, the above liquid precursor solutions were incorporated into PE separator and then heating cured at 60 °C for 12 h, resulting in PE- $x\%$ LCE@PEG ($x = 40, 50, \text{ and } 60$) gel polymer electrolytes.

2.2. Physical Characterization

Scanning electron microscopy (SEM, Hitachi S-4800) was used to observe the microstructure of the samples. A Nicolet 6700 spectrometer was used to collect Fourier transform infrared spectroscopy (FT-IR) spectra of the PEGMEA precursors and different electrolytes. Thermogravimetric analysis (TG209F1) was carried out under N₂ atmosphere with a heating rate of 10 °C min⁻¹.

2.3. Electrochemical Measurements

A Solartron 1470E electrochemical workstation was used to test electrochemical impedance spectroscopy (EIS), linear sweep voltammetry (LSV), and direct current polarization. EIS experiments were used to determine the ionic conductivity of the electrolytes using stainless steel (SS)/gel polymer electrolytes/SS symmetric cells and calculated based on Equation (1):

$$\sigma = L / (S \cdot R) \quad (1)$$

where L is the thickness, R represents the bulk resistance, and S represents the area.

The activation energy (E_a) of the electrolytes was obtained by the Arrhenius Equation (2):

$$\sigma(T) = A \exp\left(\frac{-E_a}{RT}\right) \quad (2)$$

where σ is the ionic conductivity, A is the frequency factor, R is the molar gas constant, and T is the absolute temperature. The electrochemical stability window of SS//Li cells was ascertained by linear scanning voltammetry (LSV) with a scan rate of 1 mV s^{-1} within 3–6 V. The Li^+ transference number (t_{Li^+}) of the polymeric solid electrolyte was determined by direct-current polarization on a Li//Li symmetric cell and calculated from the Bruce–Vincent–Evans Equation (3):

$$t_{\text{Li}^+} = \frac{I_{\text{ss}}(\Delta V - I_0 R_0)}{I_0\{\Delta V - I_{\text{ss}} R_{\text{ss}}\}} \quad (3)$$

where ΔV is the polarization voltage of 10 mV, I_0 is the initial current, I_{ss} is the steady-state current. R_0 and R_{ss} are the initial and steady-state interfacial resistance after the polarization process. Additionally, Li//Li symmetric batteries with various electrolytes were assembled to test the stability with lithium anode on commercial battery testing equipment (LAND Wuhan Electronics Co., Ltd., Wuhan, China).

2.4. Battery Fabrication and Evaluation

LiFePO_4 , PVDF/ LiClO_4 and Super p were mixed together with a mass ratio of 8:1:1 in N-methyl-2-pyrrolidone to prepare cathode slurry, which was coated on aluminum foil and vacuum dried at $60 \text{ }^\circ\text{C}$ for 24 h to obtain the cathode. The specific area capacity of the cathode was about 0.3 mAh cm^{-2} . The PE separator was sandwiched between the cathode and lithium metal. The gel polymer electrolyte liquid precursor solutions were injected into the cell and direct in situ solidified at $60 \text{ }^\circ\text{C}$ for 12 h to fully form PE-based gel polymer electrolytes in the battery. The charging–discharging of assembled LiFePO_4 //Li cells were tested by the commercial battery testing system (Wuhan LAND Electronics Co., Ltd.) from 2.8–3.8 V at $30 \text{ }^\circ\text{C}$, $60 \text{ }^\circ\text{C}$ and $80 \text{ }^\circ\text{C}$, respectively.

3. Results and Discussion

The flowable precursor solutions containing PEGMEA, LiTFSI, different amounts of LCE ($x = 40\%$, 50% , 60%) and initiator can be directly polymerized and transformed into solid-state LCE@PEG after thermally cured (Figure S1). Figure 1a displays the preparation schematic diagram of the PE- $x\%$ LCE@PEG ($x = 40\%$, 50% , 60%) gel polymer electrolytes. A $16 \text{ }\mu\text{m}$ -thick PE separator is selected as skeleton, which can be completely infiltrated by the transparent and flowable precursor solution. After in situ thermal curing, PE- $x\%$ LCE@PEG solid electrolytes formed. Figure 1b exhibits the FT-IR absorption spectra of PEGMEA, PEGMEA@LCE, PEG, PE- $x\%$ LCE@PEG ($x = 40, 50, \text{ and } 60$) electrolytes. Clearly, the C=C stretching vibration of acrylate group in PEGMEA at $1600\text{--}1690 \text{ cm}^{-1}$ disappears after in situ polymerization. Moreover, the C=O in the gel membrane guarantees a strong interaction with the liquid electrolyte. Figure 1c shows the TG curves of PEG, PE, PE@PEG, PE- 50% LCE@PEG and LCE. The LCE evaporates rapidly at relatively low temperature and the weight loss reaches up to 41.88% when the temperature increases to $100 \text{ }^\circ\text{C}$. In contrast, the weight loss of PE- 50% LCE@PEG is nearly zero at $100 \text{ }^\circ\text{C}$, indicating that the liquid electrolytes have been effectively immobilized in the polymerized PEG matrix and become thermally stable. Furthermore, PEG is thermally stable and its decomposition temperature can reach about $300 \text{ }^\circ\text{C}$. By further incorporating with the PE separator, the PE- 50% LCE@PEG gel polymer electrolyte exhibits good thermal stability at high temperature.

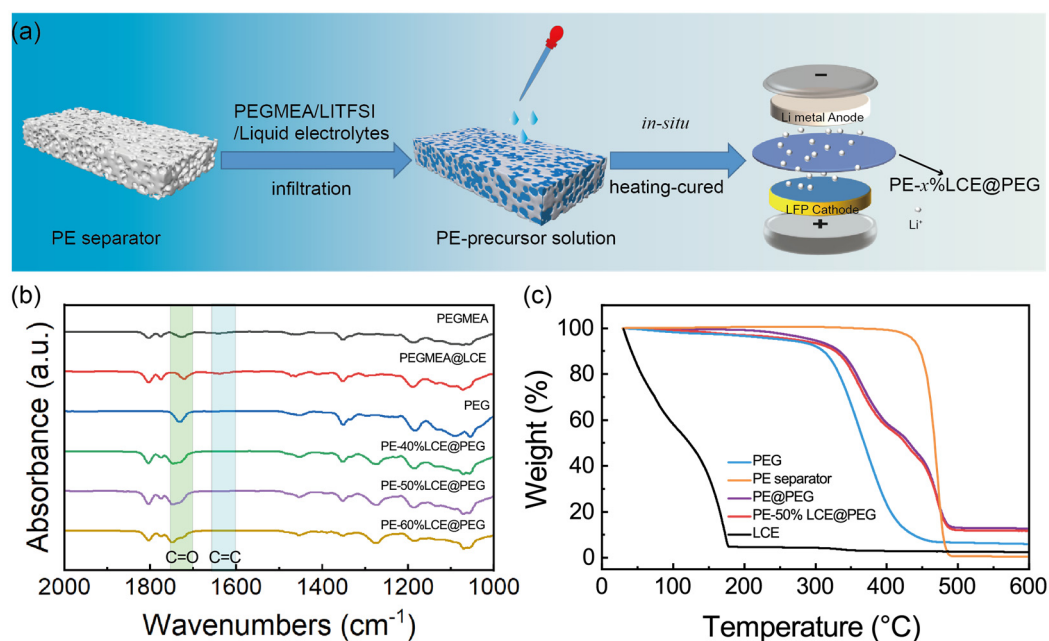


Figure 1. (a) Schematic diagram of the preparation process of PE–x%LCE@PEG via in situ polymerization. (b) FT–IR adsorption spectra of monomers and polymers. (c) TGA curves of monomers and polymers.

The morphology of PE and PE–x%LCE@PEG ($x = 40, 50,$ and 60) gel polymer electrolytes were observed by SEM. As shown in Figure 2a, the surface of the pristine PE separator shows a porous structure, which can well accommodate the precursor solution before heating curing. After in situ polymerization, the pores in PE separator store LCE@PEG well to form a gel polymer electrolyte, and the surface of the electrolyte is uniform and flat (Figure 2b and Figure S2). The thickness of the PE–50% LCE@PEG electrolyte is about $18 \mu\text{m}$ with a dense structure (Figure 2c).

The ionic conductivity of gel polymer electrolytes is measured by EIS tests (Figure S3), showing 1.21×10^{-4} , 1.73×10^{-4} , and $2.11 \times 10^{-4} \text{ S cm}^{-1}$ for PE–x%LCE@PEG ($x = 40, 50,$ and 60) at $60 \text{ }^\circ\text{C}$, respectively. The activation energies of PE–x%LCE@PEG ($x = 40, 50,$ and 60) are calculated to be 0.286, 0.281, and 0.22 eV, respectively (Figure 3a). Based on LSV testing (Figure 3b), no obvious oxidation peak for the PE–x%LCE@PEG was observed until 4.3 V vs. Li/Li⁺, which is slightly higher than that of the liquid carbonate electrolyte at 4.1 V (Figure S4). The higher electrochemical window can be ascribed to the strong interaction between the C=O groups of PEGMEA and the anions in the electrolytic salt [19,33]. Moreover, the t_{Li^+} values for PE–x%LCE@PEG ($x = 40, 50,$ and 60) gel polymer electrolytes are 0.415, 0.425, and 0.5, respectively (Figures 3c and S5), exceeding those of commercial liquid electrolytes (0.2–0.4) [34]. The high t_{Li^+} could be due to the C=O groups in the PE–x%LCE@PEG ($x = 40, 50,$ and 60) gel polymer electrolytes limiting the movement of anions, which could further reduce the concentration polarization and improve the performance of the cells [35–37]. The electrochemical stability of gel polymer electrolytes with lithium metal anode is further investigated in Li/Li symmetric cells. The critical current densities of PE–x%LCE@PEG ($x = 40, 50,$ and 60) are 1.1, 1.1, and 0.9 mA cm^{-2} , respectively (Figure 3d), indicating the PE–x%LCE@PEG ($x = 40, 50,$ and 60) gel polymer electrolytes possess good ability to inhibit lithium dendrites [38]. In addition, the long-term cyclic performances of Li//Li symmetric cells employing PE–x%LCE@PEG ($x = 40, 50,$ and 60) and LCE are shown Figure 3e and Figure S6. Clearly, PE–50%LCE@PEG gel polymer electrolyte displays the best cycling stability up to 1200 h at 0.1 mA cm^{-2} and 0.1 mAh cm^{-2} . The symmetrical cell with LCE suffers a short circuit after 875 h. The excellent interfacial stability is due to the confinement of polymer to the liquid phase,

which reduces the interfacial reactions between lithium metal and reactive electrolyte components [39].

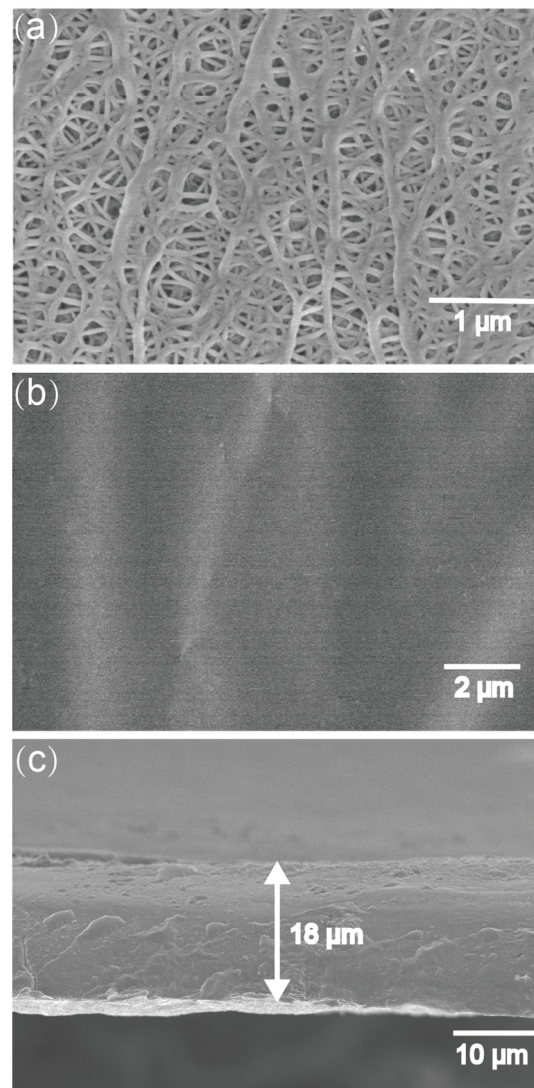


Figure 2. SEM images of (a) PE and (b) PE–50%LCE@PEG gel polymer electrolyte. (c) Cross–section SEM image of PE–50%LCE@PEG gel polymer electrolyte.

To demonstrate the feasibility of PE– $x\%$ LCE@PEG ($x = 40, 50,$ and 60) gel polymer electrolytes in rechargeable lithium metal batteries, $\text{LiFePO}_4//\text{Li}$ cells were assembled employing PE– $x\%$ LCE@PEG ($x = 40, 50,$ and 60) and LCE, as shown in Figures 4a and S7. The PE–50%LCE@PEG cell shows excellent cycling stability over 150 cycles with no capacity decay at 0.5 C under 60 °C. However, the LCE–based cell shows dramatic decrease in capacity after 30 cycles under the same conditions. Furthermore, the rate capabilities of $\text{LiFePO}_4/\text{PE}–50\%\text{LCE@PEG}$ cells were assessed at various current densities from 2.8–3.8 V (Figure 4b). The reversible capacities for PE–50%LCE@PEG cells are 164.8, 165, 160, 157, 152, 142, 63.6 mA h g^{-1} at 0.1 C, 0.2 C, 0.5 C, 1 C, 2 C, 3 C, and 5 C, respectively. The corresponding charge–discharge curves are presented in Figure 4c. With the increase of current density, the discharge voltage plateau decreases slowly without serious polarization until 3 C.

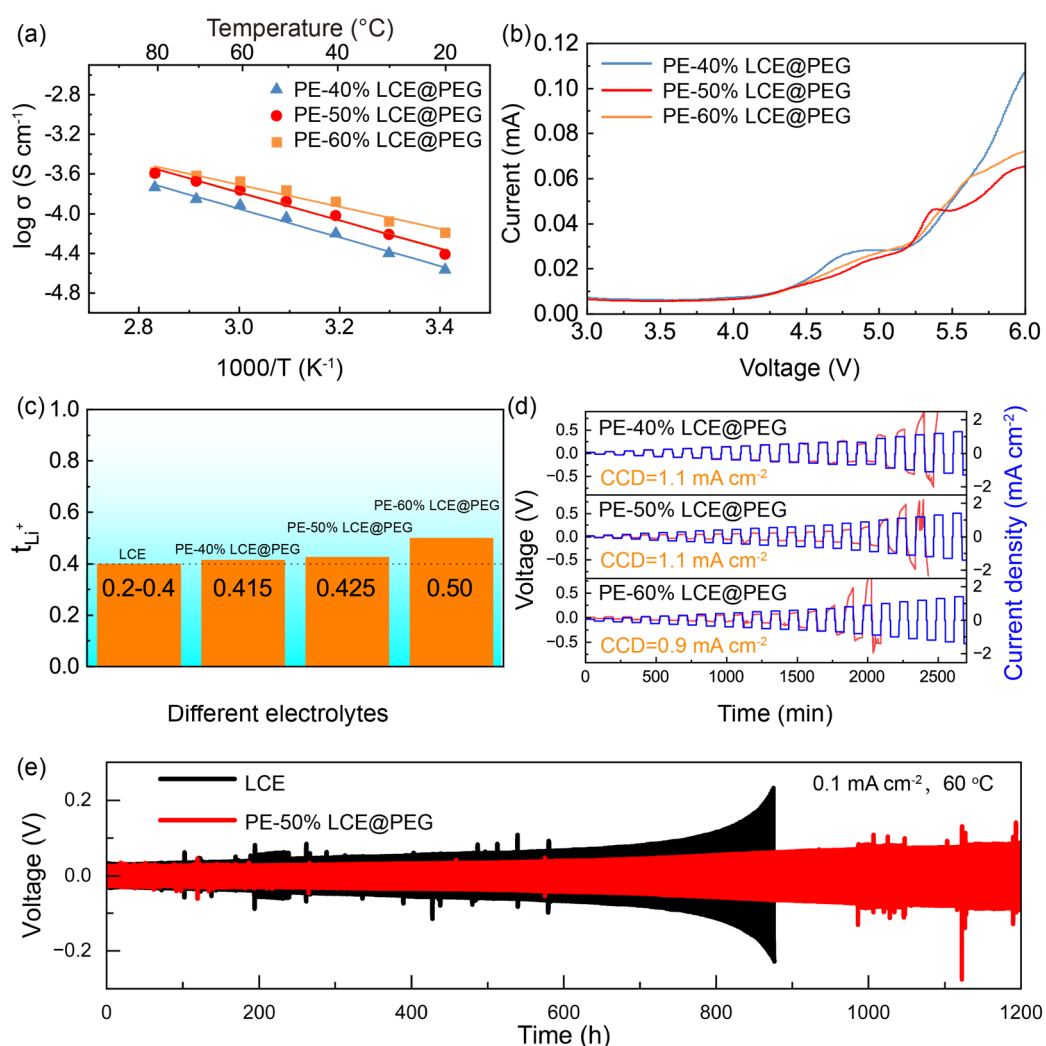


Figure 3. (a) Arrhenius plots of PE- x %LCE@PEG ($x = 40, 50,$ and 60) gel polymer electrolytes. (b) Linear sweep voltammetry of PE- x %LCE@PEG ($x = 40, 50,$ and 60) gel polymer electrolytes. (c) Li⁺ transference number comparison of LCE and PE- x %LCE@PEG ($x = 40, 50,$ and 60) gel polymer electrolytes. (d) Critical current density test of Li/PE- x %LCE@PEG ($x = 40, 50,$ and 60)/Li cells at 60 °C. (e) Long-term cyclic performances of Li//Li symmetrical cells using the LCE and PE-50%LCE@PEG gel polymer electrolytes at 0.1 mA cm⁻² and 0.1 mAh cm⁻² under 60 °C.

In addition, the cyclic performances of LiFePO₄/PE- x %LCE@PEG/Li cells and LiFePO₄/LCE/Li cells at 0.5 C under 80 °C are also evaluated, as shown in Figures 4d and S8. For the commercial liquid electrolyte-based cell, it is difficult to operate at a high temperatures of 80 °C for a long cycle life [40]. Nevertheless, the PE-50%LCE@PEG based cell can stably cycle for 100 cycles at 0.5 C under 80 °C, exhibiting a reversible discharging specific capacity of 158.5 mA h g⁻¹ at the 100th cycle with a capacity retention of 98.87%. Moreover, the LiFePO₄//Li battery with the PE-50%LCE@PEG electrolyte also possesses outstanding electrochemical performances under 0.5 C at 30 °C, showing a comparable performance with LCE-based cell (Figure S9). Furthermore, the lithium anode of the LiFePO₄/PE-50%LCE@PEG/Li cell after cycling shows a smooth and compact surface without cracks, and few lithium dendrites are observed (Figure S10). However, after cycling, the lithium anode of LiFePO₄/LCE/Li cell becomes rough and full of dendrites.

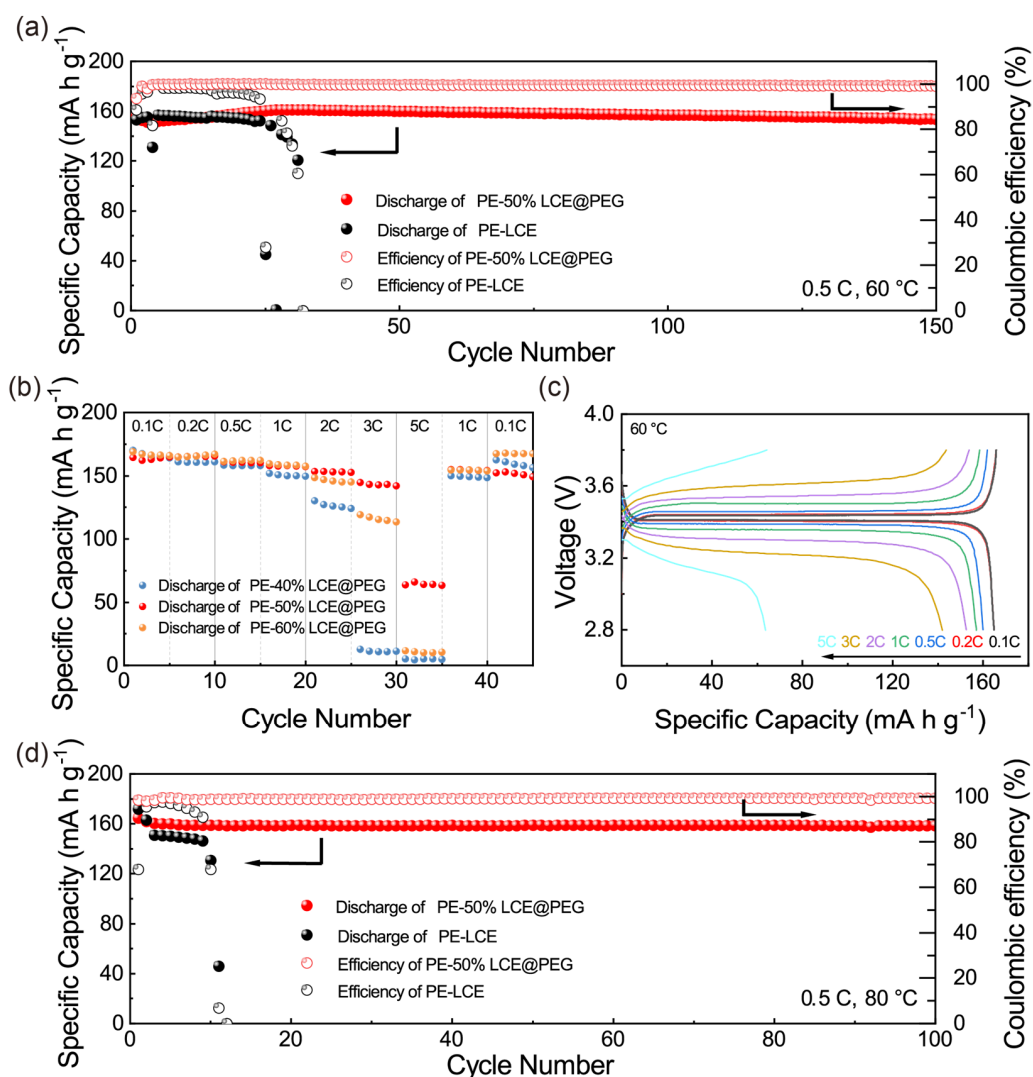


Figure 4. (a) Cyclic performances of the LiFePO₄//Li cells using PE–50%LCE@PEG and LCE under 0.5 C at 60 °C. (b) Rate capability of the LiFePO₄//Li batteries using PE–*x*%LCE@PEG (*x* = 40, 50, and 60) electrolytes at different rates at 60 °C. (c) Charge–discharge voltage profiles of LiFePO₄//Li battery using PE–50%LCE@PEG electrolyte at different rate under 60 °C. (d) Cyclic performances of the LiFePO₄//Li batteries using PE–50%LCE@PEG and LCE electrolyte under 0.5 C at 80 °C.

Furthermore, a series of flexibility and safety tests were performed on the LiFePO₄/PE–50%LCE@PEG/Li pouch cells. As shown in Figure 5, the pouch batteries with PE–50%LCE@PEG can continuously light up the yellow LED in the flat state, folded state, several fold and even cut, which displays the good reliability and safety of PE–50%LCE@PEG for flexible solid–state lithium batteries.

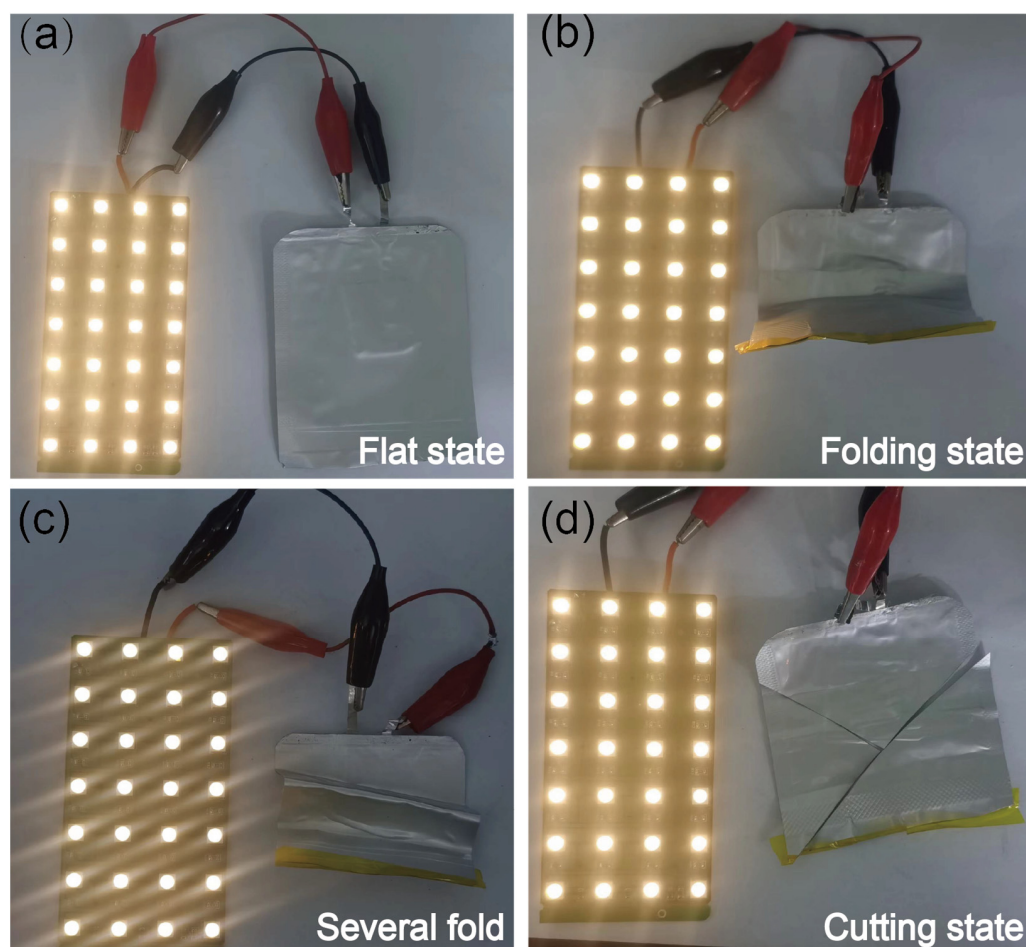


Figure 5. Optical images of the LED lamp powered by the pouch cell in various states: (a) flat state; (b) folding state; (c) several fold; (d) cutting state.

4. Conclusions

A series of PE- $x\%$ LCE@PEG ($x = 40, 50,$ and 60) gel polymer electrolytes were successfully synthesized to realize high-temperature solid-state lithium batteries. The PE-50% LCE@PEG gel polymer electrolyte shows a high ionic conductivity of $1.73 \times 10^{-4} \text{ S cm}^{-1}$ at $60 \text{ }^\circ\text{C}$ with a high Li^+ transference number of 0.425. The critical current density of PE-50%LCE@PEG gel polymer electrolyte-based Li/Li symmetric cell is up to 1.1 mA cm^{-2} , and the cell exhibits cycling stability for 1200 h at 0.1 mA cm^{-2} and 0.1 mAh cm^{-2} . The assembled $\text{LiFePO}_4/\text{PE}-50\%\text{LCE@PEG}/\text{Li}$ solid-state batteries show outstanding cycling stability with no capacity decay over 150 cycles at 0.5 C under $60 \text{ }^\circ\text{C}$. In addition, the cell exhibits a high initial reversible capacity of $160.3 \text{ mA h g}^{-1}$ under a higher temperature of $80 \text{ }^\circ\text{C}$ at 0.5 C and exhibits excellent cycling stability for 100 cycles, demonstrating promising potential application for high-temperature solid-state lithium metal batteries.

Supplementary Materials: The following supporting information can be downloaded at: <https://www.mdpi.com/article/10.3390/batteries9010028/s1>, Figure S1: Optical images of PEGMEA, LiTFSI and initiator with varied amounts of LCE before (a) and after (b) the polymerization process. Figure S2. SEM images of (a) PE-40%LCE@PEG and (b) PE-60%LCE@PEG gel polymer electrolytes. Figure S3. EIS plots of PE- $x\%$ LCE@PEG ($x =$ (a) 40, (b) 50, and (c) 60) gel polymer electrolytes at different temperatures ($20\sim 100 \text{ }^\circ\text{C}$). Figure S4. Linear sweep voltammetry of LCE. Figure S5 Chronoamperometry of (a) Li/PE-40%LCE@PEG/Li, (b) Li/PE-50%LCE@PEG/Li, (c) Li/PE-60%LCE@PEG/Li symmetric cells at ambient temperature. The insets are the alternate current impedance spectra before and after polarization. Figure S6. Long-term cycling of symmetrical Li cells using the PE-40%LCE@PEG and PE-60%LCE@PEG electrolytes at 0.1 mA cm^{-2} and

0.1 mAh cm⁻² under 60 °C. Figure S7. Cyclic performances of the LiFePO₄//Li batteries assembled with PE–40%LCE@PEG and PE–60%LCE@PEG under 0.5 C rate and 60 °C. Figure S8. Cyclic performances of the LiFePO₄//Li batteries assembled with PE–40%LCE@PEG and PE–60%LCE@PEG under 0.5 C rate and 80 °C. Figure S9. Cyclic performances of the LiFePO₄//Li battery with LCE and PE–*x*%LCE@PEG (*x* = 40, 50, and 60) electrolytes under 0.5 C rate and 30 °C. Figure S10. SEM images of the Li metal taken from (a) bare lithium, (b) LiFePO₄/PE–50%LCE@PEG/Li cell after 100 cycles under 0.5 C at 60 °C, (c) LiFePO₄/LCE/Li cell after 25 cycles under 0.5C at 60 °C.

Author Contributions: Conceptualization, X.X. and X.Y.; methodology, J.M. and Z.W.; validation, J.M., Z.W., J.W. and Z.G.; formal analysis, J.M., J.W. and Z.G.; investigation, J.M.; resources, X.Y.; data curation, J.M.; writing—original draft preparation, J.M.; writing—review and editing, X.Y.; visualization, J.M.; supervision, X.Y.; project administration, X.Y.; funding acquisition, X.Y. All authors have read and agreed to the published version of the manuscript.

Funding: The work was supported by the National Key R&D Program of China (Grant no. 2022YFB-3807700), the National Natural Science Foundation of China (Grant no. U1964205, U21A2075, 51872303, 51902321, 52172253, 52102326), Ningbo S&T Innovation 2025 Major Special Programme (Grant No. 2019B10044, 2021Z122), Zhejiang Provincial Key R&D Program of China (Grant No. 2022C01072), Jiangsu Provincial S&T Innovation Special Programme for carbon peak and carbon neutrality (Grant No. BE2022007) and Youth Innovation Promotion Association CAS (Y2021080).

Data Availability Statement: The data presented in this study are available upon request from the corresponding author.

Conflicts of Interest: The authors declare no conflict of interest.

References

1. Yamada, Y.; Furukawa, K.; Sodeyama, K.; Kikuchi, K.; Yaegashi, M.; Tateyama, Y.; Yamada, A. Unusual Stability of Acetonitrile-Based Superconcentrated Electrolytes for Fast-Charging Lithium-Ion Batteries. *J. Am. Chem. Soc.* **2014**, *136*, 5039–5046. [[CrossRef](#)] [[PubMed](#)]
2. Goodenough, J.B.; Park, K.S. The Li-Ion Rechargeable Battery: A Perspective. *J. Am. Chem. Soc.* **2013**, *135*, 1167–1176. [[CrossRef](#)] [[PubMed](#)]
3. Van Noorden, R. A BETTER BATTERY. *Nature* **2014**, *507*, 26–28. [[CrossRef](#)]
4. Voropaeva, D.Y.; Safronova, E.Y.; Novikova, S.A.; Yaroslavtsev, A.B. Recent progress in lithium-ion and lithium metal batteries. *Mendeleev Commun.* **2022**, *32*, 287–297. [[CrossRef](#)]
5. Guo, Y.; Wu, S.; He, Y.-B.; Kang, F.; Chen, L.; Li, H.; Yang, Q.-H. Solid-state lithium batteries: Safety and prospects. *eScience* **2022**, *2*, 138–163. [[CrossRef](#)]
6. Wang, Z.J.; Wang, Y.Y.; Zhang, Z.H.; Chen, X.W.; Lie, W.; He, Y.B.; Zhou, Z.; Xia, G.L.; Guo, Z.P. Building Artificial Solid-Electrolyte Interphase with Uniform Intermolecular Ionic Bonds toward Dendrite-Free Lithium Metal Anodes. *Adv. Funct. Mater.* **2020**, *30*, 2002414. [[CrossRef](#)]
7. Tarascon, J.M.; Armand, M. Issues and challenges facing rechargeable lithium batteries. *Nature* **2001**, *414*, 359–367. [[CrossRef](#)] [[PubMed](#)]
8. Hu, Z.L.; Xian, F.; Guo, Z.Y.; Lu, C.L.; Du, X.F.; Cheng, X.Y.; Zhang, S.; Dong, S.M.; Cui, G.L.; Chen, L.Q. Nonflammable Nitrile Deep Eutectic Electrolyte Enables High-Voltage Lithium Metal Batteries. *Chem. Mater.* **2020**, *32*, 3405–3413. [[CrossRef](#)]
9. Xu, K. Nonaqueous liquid electrolytes for lithium-based rechargeable batteries. *Chem. Rev.* **2004**, *104*, 4303–4417. [[CrossRef](#)] [[PubMed](#)]
10. Pieczonka, N.P.W.; Borgel, V.; Ziv, B.; Leifer, N.; Dargel, V.; Aurbach, D.; Kim, J.H.; Liu, Z.Y.; Huang, X.S.; Krachkovskiy, S.A.; et al. Lithium Polyacrylate (LiPAA) as an Advanced Binder and a Passivating Agent for High-Voltage Li-Ion Batteries. *Adv. Energy Mater.* **2015**, *5*, 1501008. [[CrossRef](#)]
11. Yang, C.P.; Yin, Y.X.; Zhang, S.F.; Li, N.W.; Guo, Y.G. Accommodating lithium into 3D current collectors with a submicron skeleton towards long-life lithium metal anodes. *Nat. Commun.* **2015**, *6*, 8058. [[CrossRef](#)]
12. Wood, S.M.; Pham, C.H.; Rodriguez, R.; Nathan, S.S.; Dolocan, A.D.; Celio, H.; de Souza, J.P.; Klavetter, K.C.; Heller, A.; Mullins, C.B. K⁺ Reduces Lithium Dendrite Growth by Forming a Thin, Less-Resistive Solid Electrolyte Interphase. *ACS Energy Lett.* **2016**, *1*, 414–419. [[CrossRef](#)]
13. Zhu, Z.Q.; Chen, X.D. Artificial interphase engineering of electrode materials to improve the overall performance of lithium-ion batteries. *Nano Res.* **2017**, *10*, 4115–4138. [[CrossRef](#)]
14. Chi, S.S.; Liu, Y.C.; Song, W.L.; Fan, L.Z.; Zhang, Q. Prestoring Lithium into Stable 3D Nickel Foam Host as Dendrite-Free Lithium Metal Anode. *Adv. Funct. Mater.* **2017**, *27*, 1700348. [[CrossRef](#)]

15. Deng, K.R.; Zeng, Q.G.; Wang, D.; Liu, Z.; Wang, G.X.; Qiu, Z.P.; Zhang, Y.F.; Xiao, M.; Meng, Y.Z. Nonflammable organic electrolytes for high-safety lithium-ion batteries. *Energy Storage Mater.* **2020**, *32*, 425–447. [[CrossRef](#)]
16. Shen, X.; Zhang, X.; Ding, F.; Huang, J.; Xu, R.; Chen, X.; Yan, C.; Su, F.; Chen, C.; Liu, X.; et al. Advanced Electrode Materials in Lithium Batteries: Retrospect and Prospect. *Energy Mater. Adv.* **2021**, *2021*, 1205324. [[CrossRef](#)]
17. Zhao, B.L.; Ma, L.X.; Wu, K.; Cao, M.X.; Xu, M.G.; Zhang, X.X.; Liu, W.; Chen, J.T. Asymmetric double-layer composite electrolyte with enhanced ionic conductivity and interface stability for all-solid-state lithium metal batteries. *Chin. Chem. Lett.* **2021**, *32*, 125–131. [[CrossRef](#)]
18. Zheng, J.; Tang, M.X.; Hu, Y.Y. Lithium Ion Pathway within $\text{Li}_7\text{La}_3\text{Zr}_2\text{O}_{12}$ -Polyethylene Oxide Composite Electrolytes. *Angew. Chem.-Int. Ed.* **2016**, *55*, 12538–12542. [[CrossRef](#)]
19. Wang, Z.Y.; Shen, L.; Deng, S.G.; Cui, P.; Yao, X.Y. 10 μm -Thick High-Strength Solid Polymer Electrolytes with Excellent Interface Compatibility for Flexible All-Solid-State Lithium-Metal Batteries. *Adv. Mater.* **2021**, *33*, 2100353. [[CrossRef](#)] [[PubMed](#)]
20. Cheng, J.; Zhang, H.; Li, D.; Li, Y.; Zeng, Z.; Ji, F.; Wei, Y.; Xu, X.; Sun, Q.; Wang, S.; et al. Agglomeration-Free and Air-Inert Garnet for Upgrading PEO/Garnet Composite Solid State Electrolyte. *Batteries* **2022**, *8*, 141. [[CrossRef](#)]
21. Zhang, X.L.; Zhao, S.Y.; Fan, W.; Wang, J.N.; Li, C.J. Long cycling, thermal stable, dendrites free gel polymer electrolyte for flexible lithium metal batteries. *Electrochim. Acta* **2019**, *301*, 304–311. [[CrossRef](#)]
22. Zhou, H.Y.; Liu, H.D.; Li, Y.J.; Yue, X.J.; Wang, X.F.; Gonzalez, M.; Meng, Y.S.; Liu, P. In situ formed polymer gel electrolytes for lithium batteries with inherent thermal shutdown safety features. *J. Mater. Chem. A* **2019**, *7*, 16984–16991. [[CrossRef](#)]
23. Zhang, S.Z.; Xia, X.H.; Xie, D.; Xu, R.C.; Xu, Y.J.; Xia, Y.; Wu, J.B.; Yao, Z.J.; Wang, X.L.; Tu, J.P. Facile interfacial modification via in-situ ultraviolet solidified gel polymer electrolyte for high-performance solid-state lithium ion batteries. *J. Power Sources* **2019**, *409*, 31–37. [[CrossRef](#)]
24. Xu, D.; Su, J.M.; Jin, J.; Sun, C.; Ruan, Y.D.; Chen, C.H.; Wen, Z.Y. In Situ Generated Fireproof Gel Polymer Electrolyte with $\text{Li}_6.4\text{Ga}_0.2\text{La}_3\text{Zr}_2\text{O}_{12}$ As Initiator and Ion-Conductive Filler. *Adv. Energy Mater.* **2019**, *9*, 1900611. [[CrossRef](#)]
25. Cho, Y.G.; Hwang, C.; Cheong, D.S.; Kim, Y.S.; Song, H.K. Gel/Solid Polymer Electrolytes Characterized by In Situ Gelation or Polymerization for Electrochemical Energy Systems. *Adv. Mater.* **2019**, *31*, 1804909. [[CrossRef](#)] [[PubMed](#)]
26. Kim, D.; Liu, X.; Yu, B.Z.; Mateti, S.; O'Dell, L.A.; Rong, Q.Z.; Chen, Y. Amine-Functionalized Boron Nitride Nanosheets: A New Functional Additive for Robust, Flexible Ion Gel Electrolyte with High Lithium-Ion Transference Number. *Adv. Funct. Mater.* **2020**, *30*, 1910813. [[CrossRef](#)]
27. Liu, F.Q.; Wang, W.P.; Yin, Y.X.; Zhang, S.F.; Shi, J.L.; Wang, L.; Zhang, X.D.; Zheng, Y.; Zhou, J.J.; Li, L.; et al. Upgrading traditional liquid electrolyte via in situ gelation for future lithium metal batteries. *Sci. Adv.* **2018**, *4*, eaat5383. [[CrossRef](#)]
28. Liu, M.; Wang, Y.; Li, M.; Li, G.Q.; Li, B.; Zhang, S.T.; Ming, H.; Qiu, J.Y.; Chen, J.H.; Zhao, P.C. A new composite gel polymer electrolyte based on matrix of PEGDA with high ionic conductivity for lithium-ion batteries. *Electrochim. Acta* **2020**, *354*, 136622. [[CrossRef](#)]
29. Zhao, Q.; Liu, X.T.; Stalin, S.; Khan, K.; Archer, L.A. Solid-state polymer electrolytes with in-built fast interfacial transport for secondary lithium batteries. *Nat. Energy* **2019**, *4*, 365–373. [[CrossRef](#)]
30. Liu, X.C.; Ding, G.L.; Zhou, X.H.; Li, S.Z.; He, W.S.; Chai, J.C.; Pang, C.G.; Liu, Z.H.; Cui, G.L. An interpenetrating network poly(diethylene glycol carbonate)-based polymer electrolyte for solid state lithium batteries. *J. Mater. Chem. A* **2017**, *5*, 11124–11130. [[CrossRef](#)]
31. Zhou, Z.X.; Feng, Y.Y.; Wang, J.L.; Liang, B.; Li, Y.H.; Song, Z.X.; Itkis, D.M.; Song, J.X. A robust, highly stretchable ion-conductive skin for stable lithium metal batteries. *Chem. Eng. J.* **2020**, *396*, 125254. [[CrossRef](#)]
32. Fan, W.; Li, N.W.; Zhang, X.L.; Zhao, S.Y.; Cao, R.; Yin, Y.Y.; Xing, Y.; Wang, J.N.; Guo, Y.G.; Li, C.J. A Dual-Salt Gel Polymer Electrolyte with 3D Cross-Linked Polymer Network for Dendrite-Free Lithium Metal Batteries. *Adv. Sci.* **2018**, *5*, 1800559. [[CrossRef](#)] [[PubMed](#)]
33. Wang, Q.Y.; Xu, X.Q.; Hong, B.; Bai, M.H.; Li, J.; Zhang, Z.; Lai, Y.Q. Molecular engineering of a gel polymer electrolyte via in-situ polymerization for high performance lithium metal batteries. *Chem. Eng. J.* **2022**, *428*, 131331. [[CrossRef](#)]
34. Diederichsen, K.M.; McShane, E.J.; McCloskey, B.D. Promising Routes to a High Li^+ Transference Number Electrolyte for Lithium Ion Batteries. *ACS Energy Lett.* **2017**, *2*, 2563–2575. [[CrossRef](#)]
35. Wang, Y.; Fu, L.; Shi, L.; Wang, Z.; Zhu, J.; Zhao, Y.; Yuan, S. Gel Polymer Electrolyte with High Li^+ Transference Number Enhancing the Cycling Stability of Lithium Anodes. *ACS Appl. Mater. Interfaces* **2019**, *11*, 5168–5175. [[CrossRef](#)]
36. Xu, H.; Xie, J.; Liu, Z.; Wang, J.; Deng, Y. Carbonyl-coordinating polymers for high-voltage solid-state lithium batteries: Solid polymer electrolytes. *MRS Energy Sustain.* **2020**, *7*, 2. [[CrossRef](#)]
37. Lin, Z.; Guo, X.; Wang, Z.; Wang, B.; He, S.; O'Dell, L.A.; Huang, J.; Li, H.; Yu, H.; Chen, L. A wide-temperature superior ionic conductive polymer electrolyte for lithium metal battery. *Nano Energy* **2020**, *73*, 104786. [[CrossRef](#)]
38. Shen, L.; Deng, S.G.; Jiang, R.R.; Liu, G.Z.; Yang, J.; Yao, X.Y. Flexible composite solid electrolyte with 80 wt% $\text{Na}_3.4\text{Zr}_1.9\text{Zn}_0.1\text{Si}_2.2\text{P}_0.8\text{O}_{12}$ for solid-state sodium batteries. *Energy Storage Mater.* **2022**, *46*, 175–181. [[CrossRef](#)]

39. Zhou, W.D.; Wang, S.F.; Li, Y.T.; Xin, S.; Manthiram, A.; Goodenough, J.B. Plating a Dendrite-Free Lithium Anode with a Polymer/Ceramic/Polymer Sandwich Electrolyte. *J. Am. Chem. Soc.* **2016**, *138*, 9385–9388. [[CrossRef](#)]
40. Chang, Z.; Yang, H.J.; Zhu, X.Y.; He, P.; Zhou, H.S. A stable quasi-solid electrolyte improves the safe operation of highly efficient lithium-metal pouch cells in harsh environments. *Nat. Commun.* **2022**, *13*, 1510. [[CrossRef](#)]

Disclaimer/Publisher’s Note: The statements, opinions and data contained in all publications are solely those of the individual author(s) and contributor(s) and not of MDPI and/or the editor(s). MDPI and/or the editor(s) disclaim responsibility for any injury to people or property resulting from any ideas, methods, instructions or products referred to in the content.